ACS OMEGA

Article

Cite This: ACS Omega 2019, 4, 7931−7937

http://pubs.acs.org/journal/acsodf

Fluorescence Optosensing of Triclosan by Upconversion Nanoparticles with Potassium Permanganate

Dasom Jung, Zayakhuu Gerelkhuu, Bui The Huy, and Yong-Ill Lee*

Department of Chemistry, Changwon National University, Changwon 51140, Republic of Korea

ABSTRACT: It is greatly significant to develop a simple and rapid sensing method for triclosan (TCS) because it is a widely used and a chronically toxic compound that adversely affects biological organisms and human health. This paper presents the design and development of a novel simple optosensor that uses carboxylic group-functionalized $NaYF_4$:Yb^{3+}/Er^{3+} upconversion nanoparticles (UCNPs) coated with potassium permanganate ($KMnO_4$). The sensor enables the rapid, non-autofluorescence, sensitive, and selective detection of TCS based on the "turn off−on fluorescence" technique through fluorescence resonance energy transfer. Under an near-infrared radiation excitation (980 nm), the "turn-off fluorescence" process involves the transfer of fluorescence resonance energy between the UCNPs and $KMnO_4$, whereas the "turn-on fluorescence" process occurs when $KMnO_4$ is reduced in the presence of TCS. TCS was detected by recovering the green emission of UCNPs. Under optimized conditions, the resulting sensor offered an excellent response to TCS with 0.2 μM of a limit of detection. The developed sensor showed higher selectivity to TCS than other phenolic compounds. Moreover, the analytical performance of the proposed probe was practically demonstrated to successfully monitor trace levels of TCS in samples of tap water and personal care products. The developed simple and sensitive method may offer a new approach for determining TCS in environmental applications.

1. INTRODUCTION

Triclosan (TCS) is widely used as an antimicrobial and preservative agent in household cleaners, toothpaste, soap, and plastics with a concentration ranging from 0.1 to 0.3% of product weight.[1,2] It is found in ubiquitous environments including wastewater, drinking water, soils, and living organisms.[3] However, once TCS has been released into the environment, it is considered as a toxic pollutant capable of disrupting endocrine compounds because its structure is similar to that of thyroid hormones. Moreover, TCS can kill normal bacteria by blocking the biosynthesis of lipids and causes mutated bacteria that become resistant to TCS and are more likely to survive and be reproduced.[4,5] The growing awareness of the toxicity of TCS has led to an increasing demand for the development of highly sensitive analytical methods. In recent years, several analytical methods for the determination of TCS have been developed, among which are those based on chromatography,[6−8] electrochemistry,[9,10] spectroscopy,[11−13] immunoassay,[14] and decomposition by an enzyme or radicals.[15−17] However, these methods need expensive instrumentation and complicated procedures and require highly skilled personnel. In particular, methods that use fluorescent techniques for the determination of TCS have not yet been reported. Therefore, the development of a TCS optosensor with high sensitivity and selectivity remains a challenge that has not yet been addressed.

Potassium permanganate (Mn(VII); $KMnO_4$) is a strong oxidative agent that reacts with electron-rich moieties such as phenols, anilines, and olefins. Compared with other oxidants such as ozone, chlorine, and ferrate, $KMnO_4$ has several advantages such as its relatively low cost, ease of handling, effectiveness across a wide pH range, and comparative stability.[18] In addition, the oxidation processes of antibiotics, phenolic endocrine disrupting chemicals, and organic pollutants have been demonstrated based on the reaction with Mn(VII) as an oxidant.[19,20] The reactions of Mn(VII) with certain organic compounds commonly lead to the formation of a series of intermediates such as Mn(IV) or Mn(III) depending on the nature of the ligands. Stable Mn(III) has been found to be produced by the oxidation of organic substances in the presence of certain ligands, such as phosphate, pyrophosphate, ethylenediamine tetraacetic acid, and humic acid. In addition, Mn(IV) can be aggregated by an oxidative process to form brown colloids. This is stabilized by preventing the disproportionate oxidation of $KMnO_4$ and the formation of intermediates is accelerated by the oxidation of TCS by Mn(IV).[20−22] Furthermore, Mn(VII) readily oxidizes TCS via several reactions including hydrogen abstraction, electron exchange, and direct oxygen transfer, thereby decreasing the adverse activity of TCS.[23] Jiang's group found that, during the Mn(VII)/TCS reaction, the absorption band of inherent Mn(VII) disappears from the range 490−590

Received: December 30, 2018
Accepted: April 5, 2019
Published: May 1, 2019

DOI: 10.1021/acsomega.8b03680
ACS Omega 2019, 4, 7931−7937

Scheme 1. Proposed Mechanism of "Turn Off−On" for Detection of TCS

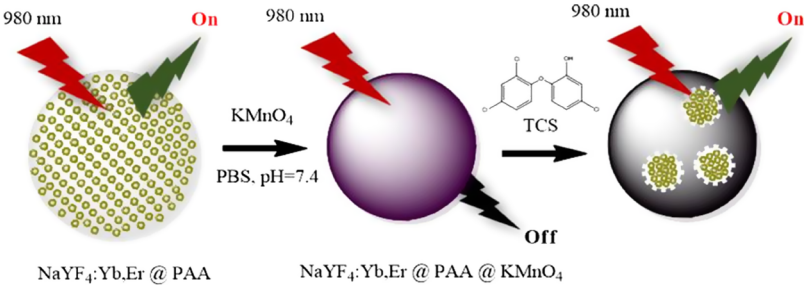

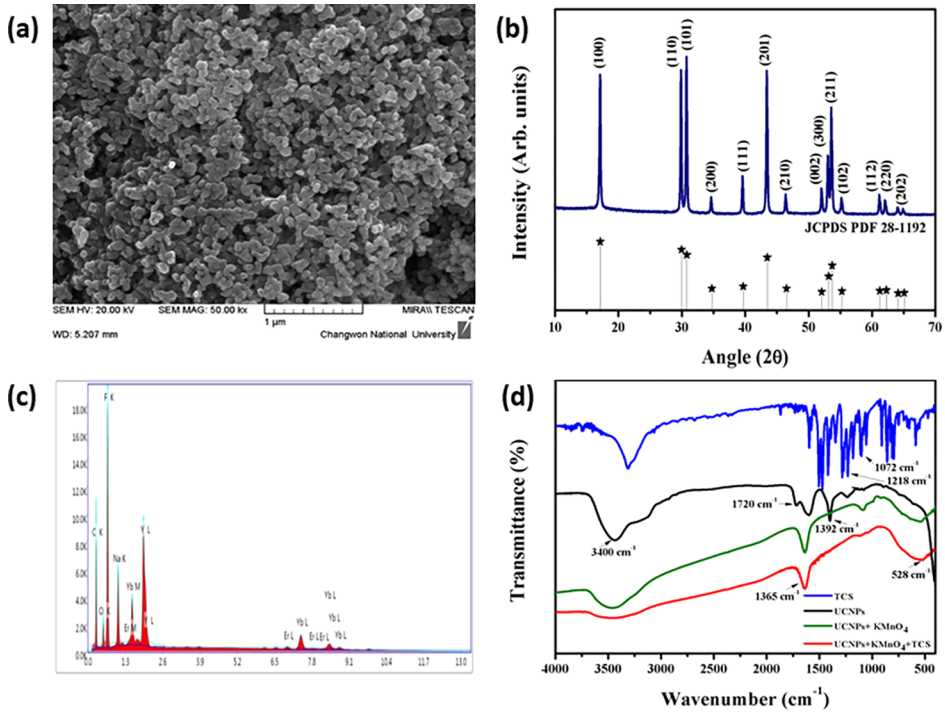

Figure 1. Characterization of PAA-functionalized $NaYF_4$:Yb^{3+}/Er^{3+} UCNPs; (a) FE-SEM image, (b) XRD pattern, (c) EDS analysis, (d) FT-IR spectra.

nm.[24] As a result, we expect $KMnO_4$ to be an excellent candidate for the detection of TCS by fluorescent materials that emit light in the blue and green bands of the visible spectrum.

Compared with other fluorescent materials such as organic fluorescent dyes and quantum dots, upconversion nanoparticles (UCNPs) that emit visible light following an excitation with near-infrared radiation (NIR) have been widely used in biological and chemical applications. In particular, the use of NIR irradiation has attractive properties, including sharp emission, low toxicity, non-autofluorescence, absence of photodamage, and deep tissue permeability.[25,26] $NaYF_4$, which has low phonon energy, is often used as the host material of the upconversion material with doping Yb^{3+} and Er^{3+}. The Yb^{3+}, Er^{3+} ions are the sensitizer and the activator, respectively. Under NIR excitation (980 nm wavelength), the fluorescent upconversion process appears when there are transfers of excited energy from Yb^{3+} ions to Er^{3+} ions. The relax process of Er^{3+} ions gives radiative transitions at the green band. The observed upconversion luminescence (UCL) spectra only originate from $NaYF_4$:Yb,Er.[27−29] Therefore, one of the advantages of the fluorescent upconversion process is non-autofluorescence from the matrix of the sample when the sample is excited by NIR wavelength.

However, UCNPs synthesized via general methods have low solubility and lack the functional groups required to react with analytes. Therefore, it is necessary to modify the surface of UCNPs to enable them to selectively detect the target materials.[30−32] Many researchers have developed UCNPs based on the fluorescence resonance energy transfer (FRET) process for sensing specific biomolecules. For example, UCNPs coated with manganese dioxide (MnO_2) nanosheets were designed for the detection of glutathione (GSH) and glucose (Glu) by using UCNPs as the donor and MnO_2 as the acceptor, which were released from UCNPs' surface in the presence of GSH and Glu.[33,34] UCNPs coated with MnO_2 indicated that the analytes could be effectively determined by controlling the fluorescence emission band. However, in their study, they used a core−shell structure, which was synthesized in an organic solvent, and either the surface of the UCNPs had to be modified such that they became hydrophilic nanoparticles or glucose oxidase was used (for sensing Glu).

In this work, we report for the first time a simple approach for the rapid and highly selective detection of TCS by using poly(acrylic acid) (PAA)-functionalized $NaYF_4$:Yb^{3+}/Er^{3+}

DOI: 10.1021/acsomega.8b03680
ACS Omega 2019, 4, 7931−7937

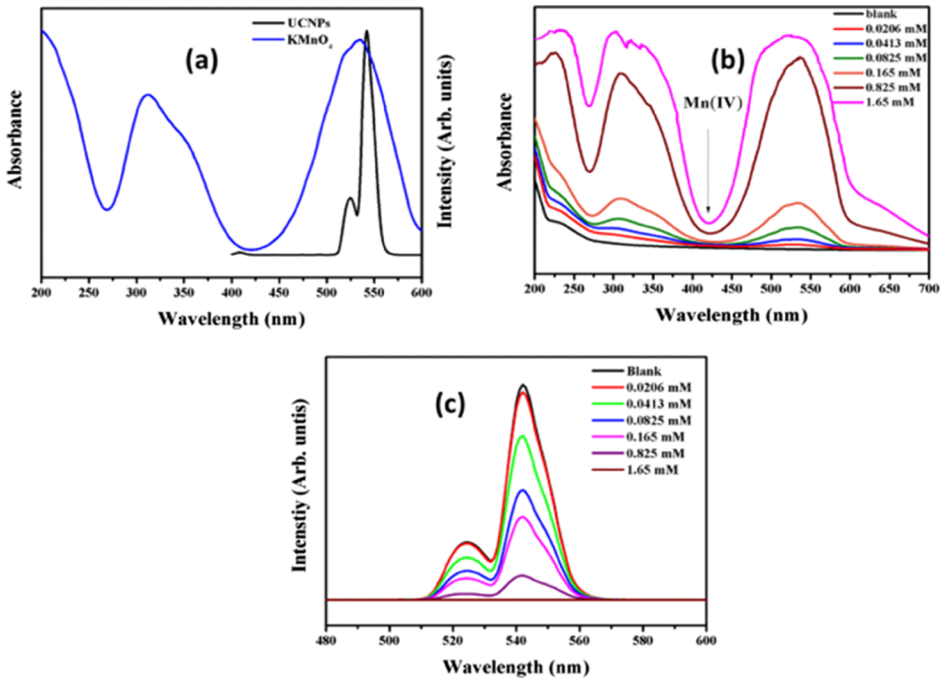

Figure 2. (a) Absorption spectrum of $KMnO_4$ (blue line) and emission of the prepared UCNPs (black line), (b) absorption spectra at various concentrations of $KMnO_4$, and (c) effect of $KMnO_4$ concentration on UCL spectra after a reaction time of 2 h.

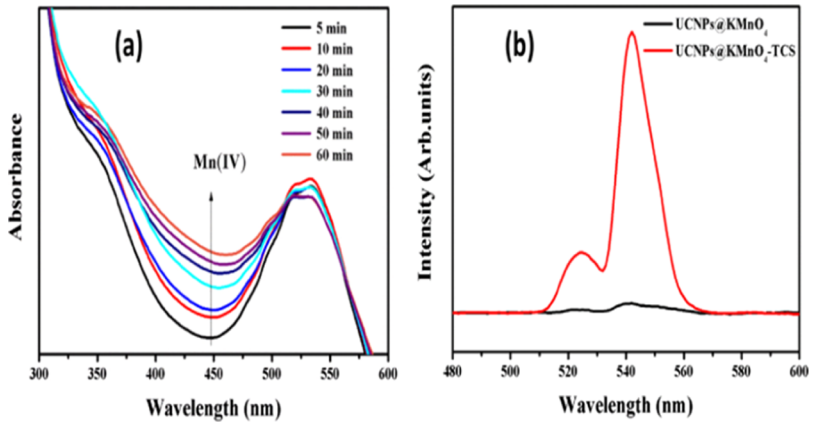

Figure 3. (a) Effect of reaction time on absorption spectra of UCNPs@$KMnO_4$ in the presence of TCS. (b) UCL spectra of UCNPs@$KMnO_4$ before (black line) and after addition of TCS (red line).

UCNPs coated with $KMnO_4$. The method was based on the FRET process that occurs in the green emission band, which was originated from the radiative transitions of Er^{3+} ions through the energy transfer process from Yb^{3+} ions. The UCNPs were synthesized via a one-step solvothermal method at 200 °C for 12 h. The PAA-functionalized $NaYF_4$:Yb^{3+}/Er^{3+} UCNPs are high soluble in aqueous solution and react with added $KMnO_4$ by electrostatic interactions. The emission of green light (500−570 nm) by NIR-excited UNCPs donor is inhibited by $KMnO_4$ (FRET acceptor) via the FRET process. Upon TCS addition, $KMnO_4$ oxidizes TCS by attacking its hydroxyl group, thereby forming MnO_2, which does not absorb 500−570 nm. Thus, FRET is disrupted, and UCNPs emit green light, as shown in Scheme 1.

2. RESULTS AND DISCUSSION

2.1. Characterization of PAA-Functionalized $NaYF_4$:Yb^{3+}/Er^{3+} UCNPs. The obtained UCNPs were characterized by field emission scanning electron microscopy (FE-SEM), X-ray diffractometry (XRD), energy-dispersive X-ray spectroscopy (EDS), and Fourier transform infrared (FT-IR), and the results are shown in Figure 1. The FE-SEM images show that the prepared UCNPs have uniform shapes and a particle size of 100 nm (Figure 1a). The XRD pattern of the sample corresponds with the referenced peak position and intensity of hexagonal $NaYF_4$ (JCPDS PDF 28-1192), confirming the formation of well-crystallized UCNPs (Figure 1b). Moreover, the EDS analysis revealed the composition of $NaYF_4$:Yb^{3+}/Er^{3+} and PAA (Figure 1c).

The functional groups on the surface of the obtained UCNP samples were identified by recording FT-IR spectra. As shown in Figure 1d (black line), a broad absorption band at 3400 cm^{-1} relates with O−H stretching vibrations. The peaks at 1720 and 1392 cm^{-1} confirm the existence of the COOH group and the carboxylate anion, respectively. Other peaks are consistent with C═C stretching at approximately 1400−1550

DOI: 10.1021/acsomega.8b03680
ACS Omega 2019, 4, 7931−7937

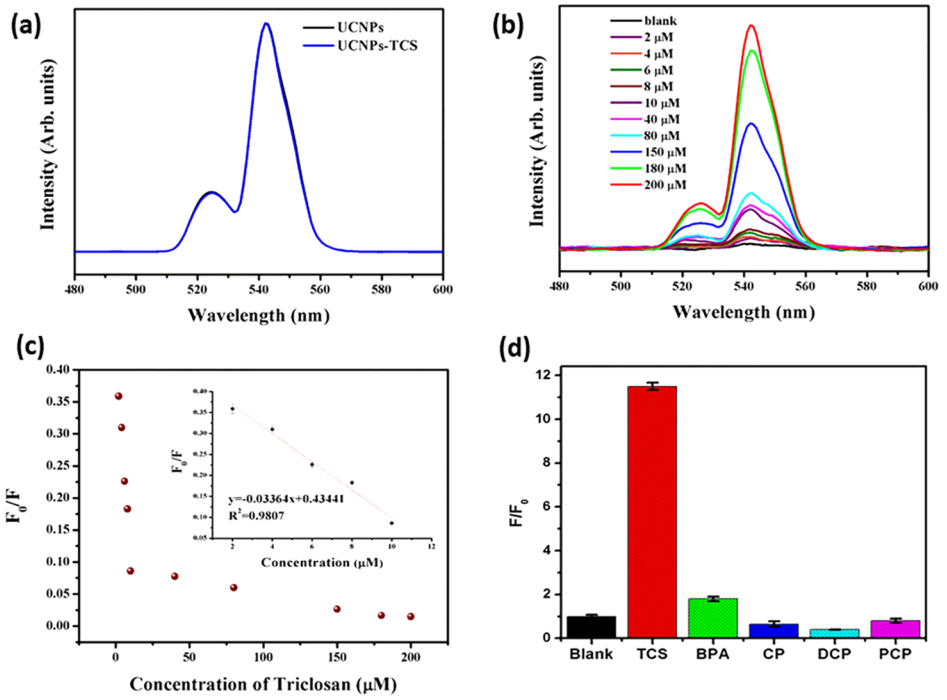

Figure 4. (a) Evaluation of UCL for UCNPs uncoated with $KMnO_4$ upon addition of TCS, (b) UCL variation of UCNPs@$KMnO_4$ at 542 nm following the addition TCS at different concentrations, (c) relationship between intensity ratio of F_0/F at 542 nm and concentration of TCS. Inset: calibration curve by plotting the UCL ratio and concentration of TCS (2, 4, 6, 8, 10 μM), (d) UCL ratio (F/F_0) of UCNPs@$KMnO_4$ after addition of various compounds at 10 μM after 60 min of incubation. F_0 and F were UCL intensity at 542 nm in the absence and presence of the compounds.

cm^{-1}. The COOH group on the surface of the UCNPs ensures good solubility and reacts with $KMnO_4$. The peak at 528 cm^{-1}, which is the Mn−O stretching vibration, confirms the existence of this bond on the UCNPs.

2.2. Fluorescent Property of UCNPs@$KMnO_4$. The UV−vis and UCL spectra of UCNPs@$KMnO_4$ show that the absorption band of $KMnO_4$ and the emission of UCNPs overlap in the region of 500−550 nm (Figure 2a). This overlap can lead to FRET from the UCNPs (as donor) to the $KMnO_4$ (as acceptor) in the green emission band to decrease the UCL intensity of the UCNPs. The effect of the $KMnO_4$ concentration on the absorbance and UCL intensity of UCNPs was assessed. We found that the absorption band appeared in the range of 400−450 nm when the concentration of $KMnO_4$ exceeded 0.825 mM (Figure 2b). This band can be related to MnO_2 because $KMnO_4$ exists as MnO_2 under neutral or slightly alkaline conditions.[23] As shown in Figure 2c, the green emission of UCNPs decreased with increasing $KMnO_4$ concentration and was completely quenched when the concentration of $KMnO_4$ reached 1.65 mM. On the basis of this result, the value of 1.65 mM $KMnO_4$ was selected for subsequent experiments.

The time dependence of the reaction between UCNP@$KMnO_4$ and TCS was studied. Figure 3a shows the absorption spectra of a mixture of UCNP@$KMnO_4$ and TCS after different reaction times. We found that the change of absorbance in the range of 500−550 nm was negligible with increasing the reaction time, whereas the nonspecific absorbance at a short range <500 nm corresponding to colloidal manganese oxides Mn(IV) gradually increased with increasing reaction time. The brown colloid Mn(IV), which was formed as the intermediate when Mn(VII) oxidizes TCS, can be observed by the naked eye. Although Mn(VII) is generally converted to the Mn(III) state when TCS is oxidized in the presence of a ligand, in the case of PBS, Mn(IV) rather than Mn(III) is formed.[20−22] Therefore, a certain amount of MnO_2 was formed and increased in the presence of TCS in the UCNPs@$KMnO_4$ solution. The UCL intensity of UCNPs was quenched by coating $KMnO_4$ because of the overlap between the absorption spectrum of $KMnO_4$ and emission spectrum of UCNPs. By adding TCS, the UCL intensity was recovered. The UCL spectra of UCNPs@$KMnO_4$ before and after adding TCS are shown in Figure 3b.

2.3. Detection on TCS-Possible Mechanisms. In this study, UCNPs@ $KMnO_4$ nanoparticles were used to detect TCS based on the "turn off−on fluorescence intensity" process. TCS oxidation by $KMnO_4$ mainly involves two pathways, which are cleavage of the ether bond of TCS by free chlorine ferrate, O_3, MnO_2, and a benzene ring-opening reaction.[23] On the basis of this information, we predicted cleavage of the ether bond because of the formation of MnO_2 during the reaction of UCNPs@$KMnO_4$, but the −OH stretching band on the FT-IR spectra (Figure 1d, red line) largely disappears after TCS is added. More significantly, the Mn−O stretching vibration at 528 cm^{-1} increased compared to UCNPs@$KMnO_4$. These results indicate that the hydroxyl group of TCS is attacked by $KMnO_4$, after which the benzene ring-opening reaction occurs. After the addition of TCS, $KMnO_4$ separated from the surface of the UCNPs. This is a result of the oxidation of TCS by $KMnO_4$. As a result, the UCNPs' surface was exposed and released emission in the green band, as shown in Figure 3b. The addition of TCS to the UCNPs@$KMnO_4$ solution strongly enhanced the green emission band of UCNPs@ $KMnO_4$ approximately 36 times upon exposure to 980 nm excitation.

On the basis of the abovementioned mechanisms, the TCS analytical performance of the proposed optosensor was investigated by measuring the recovery of the UCL intensity.

DOI: 10.1021/acsomega.8b03680
ACS Omega 2019, 4, 7931−7937

When TCS was directly added to UCNPs that have not been coated with $KMnO_4$, the UCL intensity remains unchanged, as shown in Figure 4a. However, the UCL intensity of UCNPs@$KMnO_4$ gradually increased with the addition of different TCS concentrations. The dependence of the UCL intensity of UCNPs@$KMnO_4$ on the TCS concentration is presented in Figure 4b.

The relationship between the UCL intensity and TCS concentration was estimated, as shown in Figure 4c. A calibration curve was established based on the relationship between the TCS concentration and UCL intensity F_0/F ratios (F_0 and F are the UCL intensities at 542 nm in the absence and presence of TCS, respectively), as displayed in Figure 4c. The results show that there are two linear ranges: the first one is in the range of 2−10 μM and the second one is in the range of 10−200 μM. The regression equation in the range of 2−10 μM is $F_0/F = -0.03364[TCS] + 0.43441$, where [TCS] is the concentration of TCS (μM) and the correlation coefficient is 0.9807. The detection limit (LOD) of the proposed sensor for TCS was calculated to be 0.2 μM according to the 3.3 × SD/S equation (SD is standard deviation of the signal and S is the slope of the calibration curve). The performance of the proposed method was additionally examined by comparing the results with those obtained by other methods, as shown in Table 1. Although the LOD value of the proposed method is comparable to those of electrochemical methods, the proposed optical method does not require sophisticated equipment and highly skilled personnel. Moreover, by using diluted acetone for dissolving TCS, the proposed method can be used to detect a high TCS concentration (to 200 μM).

Table 1. Comparison with Other Methods

method	LOD (μmol/L)	detection range (μmol/L)
HPLC-sorptive extraction[35]	0.002	0.001−0.4
electrochemical-polymer[36]	0.250	1−100
capillary electrophoresis-UV[37]	0.015	0.07−7
electrochemical-graphene[38]	0.6	0.6−30
electrochemical-carbon nanotube[39]	0.005	0.005−7
electrochemical-carbon NP[40]	10	1−120
electrochemical-Au/graphene[41]	0.04	0.2−14
electrochemical-multiwalled carbon nanotube[42]	0.06	0.2−6
FRET upconversion NP[a]	0.2	2−10

[a]This work.

The selectivity of the UCNPs@$KMnO_4$ optosensor was evaluated. The UCL response of UCNPs@$KMnO_4$ was assessed with compounds related to TCS, including bisphenol A (BPA), 4-chlorophenol (CP), 2,4-dichlorophenol (DCP), and pentachlorophenol (PCP) after reacting for 1 h at a concentration of 10 μM (Figure 4d). Compared to the other species, the UCL intensity was strongly recovered in the presence of TCS, showing the loss of the hydroxyl group as a consequence of the oxidation of TCS. However, all the other compounds except for PCP also have a hydroxyl group. Considering the second-order rate constants of the reaction of each of these compounds with $KMnO_4$ under neutral conditions, it is clear that the reaction of $KMnO_4$ with TCS is much faster than with the other compounds.[18] Moreover, among the substituted phenols, the oxidative reactivity of TCS with manganese oxide (Mn(IV)) is comparable or higher.[43] These results show the high sensitivity and selectivity toward TCS based on the UCNPs@$KMnO_4$ fluorescence properties.

2.4. Determination of TCS in Real Samples. To evaluate the applicability of the fluorescence sensing system, UCNPs@$KMnO_4$ was employed for the determination of TCS by analyzing tap water samples and commercially available personal care products. The tap water hand-wash samples were spiked with different amounts of TCS and the samples were analyzed to determine the TCS concentration. The results are summarized in Table 2. The recovery of TCS in tap water is 92 and 106.7, and 97 and 98% for hand-wash products with RSD < 4%, respectively. These values indicate that the proposed optosensor is satisfactory and suitable for the detection of TCS in practical applications.

Table 2. Recovery Study in Real Samples

samples	spike (μM)	found (μM)	recovery (%)	RSD (n = 3, %)
tap water	3	3.2	106.7	3.68
	5	4.6	92	3.96
hand wash	3	2.9	97	3.97
	5	4.9	98	1.79

The applicability of the proposed method was further assessed by determining the TCS in commercial toothpaste samples by the standard addition method. The results indicated that TCS levels of four different brands of toothpaste [2 g of toothpaste diluted into 1 L of distilled water (DW)] are 3.44, 9.32, 9.99, and 7.52 μM, which are comparable or similar to TCS levels compared with those with other methods.[35,36] These results confirmed that this probe demonstrates good sensitivity and accuracy to monitor TCS in real samples.

3. CONCLUSIONS

In summary, this paper presents the first demonstration that TCS can be detected based on the "turn off−on" fluorescence of UCNPs@$KMnO_4$. A possible mechanism for the determination of TCS is that the UCL intensity of UCNPs@$KMnO_4$ is quenched in the green band by an energy transfer process between UCNPs and $KMnO_4$, and then recovered again in the presence of TCS. The novel TCS sensor possesses high sensitivity and selectivity. This study confirmed that UCNPs@$KMnO_4$ is a useful probe for determining TCS and that the method is broadly applicable to the environmental field.

4. MATERIALS AND METHODS

4.1. Reagent and Materials. Ammonium fluoride (NH_4F), yttrium oxide (Y_2O_3, 99.99%), erbium oxide (Er_2O_3, 99.99%), ytterbium oxide (Yb_2O_3, 99.99%), TCS, certificated reference material (CRM), BPA, DCP, PCP, potassium permanganate ($KMnO_4$), and phosphate buffer saline (PBS, pH = 7.4) were purchased from Sigma-Aldrich. PAA (M_w = 2000) was obtained from Acros Organics. Concentrated hydrochloric acid (HCl) and ethylene glycol (EG) were obtained from Alfa Aesar. Sodium chloride (NaCl) and CP were purchased from Oriental Chemical Industries and Junsei Chemical Company, respectively. A stock solution of TCS (0.345 mM) was prepared in 5 mL of acetone solution (acetone/water = 5:95, v/v). All other reagents were of analytical grade and used as received without any further purification.

4.2. Preparation of Hydrophilic $NaYF_4$:Yb^{3+}/Er^{3+} UCNPs and Coated by $KMnO_4$. PAA-capped $NaYF_4$:Yb^{3+}/

DOI: 10.1021/acsomega.8b03680
ACS Omega 2019, 4, 7931−7937

Er^{3+} nanoparticles were synthesized using the following method.[44] Typically, NaCl (2.4 mmol), $RECl_3$ (Y:Er:Yb = 80:2:18, 0.1 mmol), PAA 0.3 g were dissolved in 15 mL of EG and then NH_4F (5 mmol) in 5 mL of EG was added while stirring. The resulting mixture was stirred at room temperature for 30 min and then transferred to a 30 mL Teflon-lined autoclave. The autoclave was heated at 200 °C for 12 h. After cooling to room temperature, the precipitates were separated from the mixture by centrifugation and washed with DW and ethanol several times, and dried in a vacuum oven at 50 °C overnight. The obtained UCNPs were dispersed in PBS buffer at a concentration of 0.2 mg/mL. To use the UCNPs for the detection of TCS, 1.65 mmol of $KMnO_4$ was dissolved in PBS buffer and was added to the solution of UCNPs with stirring at room temperature for 2 h. The obtained UCNPs@$KMnO_4$ samples were washed with DW for removing excess potassium, free manganese ions, and then re-dispersed in PBS buffer.

4.3. Detection of TCS. To a solution of 1.625 mL of the UCNPs coated with $KMnO_4$ (UCNPs@$KMnO_4$) were added various amounts of TCS and then filled up to 3 mL by PBS buffer (pH 7.4). The TCS concentration in this experiment was in the range of 2−200 μM. The mixture was stirred at room temperature for 1 h. After the reaction, the fluorescence intensity was recorded under an excitation wavelength of 980 nm.

4.4. Sample Preparation. The availability of the proposed sensor was assessed by studying samples of tap water, hand-wash product, and four tubes of toothpastes. The tap water samples were collected from our laboratory at Changwon National University. Before use, the water samples were filtrated by using a 0.22 μm syringe filter and maintained at 4 °C in the dark.[45] The commercial hand-wash product (0.5 g) was dissolved in 25 mL methanol with sonication for 30 min. After filtration, the solution was diluted 25-fold with DW. A stock solution of TCS (0.345 mM) was prepared by dissolving 99.89 mg of TCS in 5 mL of acetone and diluted with deionized water. Spiked samples were obtained by adding TCS solutions with different concentrations. The toothpaste samples that were analyzed to determine their TCS content were acquired at local markets. These samples were prepared by dispersing 1.25 g of toothpaste in 25 mL of DW under sonication for 15 min. The resulting suspension was diluted 25-fold with DW, and filtered by using 0.45 μm syringe filters.[46]

4.5. Characterizations. The crystal structure was determined using XRD (X'Pert PW3040/00, PANalytical; Almelo, The Netherlands) using Cu Kα (ratio Kα_2/Kα_1 = 0.5) radiation with step mode (step size 0.02). The morphology of the samples was determined by FE-SEM (CZ/MIRA II LMH, Tescan, Czech). EDS emission spectra were measured using an EDAX X-ray detector incorporated with the FE-SEM. The electron beam was accelerated at 20 kV. FT-IR spectra were obtained using a Nicolet iS10 FT-IR spectrometer (Thermo Fisher Scientific, Madison, USA). The UCL emission spectra were recorded with a fluorescence spectrophotometer (Acton SpectraPro 750-triplet grating monochromator) containing a charge coupled device detector (Princeton EEV 1024 × 1024 and PI-Max 133 controller). A 980 nm laser diode was used as an excitation source, and was placed at an angle of 45° in front of the sample holder.

AUTHOR INFORMATION

Corresponding Author

*E-mail: yilee@changwon.ac.kr.

ORCID

Yong-Ill Lee: 0000-0001-5383-9801

Author Contributions

The paper was written through contributions of all the authors. All the authors have given approval to the final version of the paper. The present work was conceived and supervised by Y.I.L, and all experimental processes and manuscript writing were performed by D.J., Z.G., and B.T.H.

Notes

The authors declare no competing financial interest.

ACKNOWLEDGMENTS

This work was supported by the Basic Science Research Program of the National Research Foundation of Korea (NRF-2017R1A2B4006388 and NRF-2017R1D1A3B03035530).

REFERENCES

(1) Rodricks, J. V.; Swenberg, J. A.; Borzelleca, J. F.; Maronpot, R. R.; Shipp, A. M. Triclosan: A critical review of the experimental data and development of margins of safety for consumer products. *Crit. Rev. Toxicol.* **2010**, *40*, 422−484.

(2) Singer, H.; Müller, S.; Tixier, C.; Pillonel, L. Triclosan: Occurrence and Fate of a Widely Used Biocide in the Aquatic Environment: Field Measurements in Wastewater Treatment Plants, Surface Waters, and Lake Sediments. *Environ. Sci. Technol.* **2002**, *36*, 4998−5004.

(3) Bedoux, G.; Roig, B.; Thomas, O.; Dupont, V.; Le Bot, B. Occurrence and toxicity of antimicrobial triclosan and by-products in the environment. *Environ. Sci. Pollut. Res.* **2012**, *19*, 1044−1065.

(4) Lee, D. G. Removal of a synthetic broad-spectrum antimicrobial agent, triclosan, in wastewater treatment systems: A short review. *Environ. Eng. Res.* **2015**, *20*, 111−120.

(5) Dann, A. B.; Hontela, A. Triclosan: environmental exposure, toxicity and mechanisms of action. *J. Appl. Toxicol.* **2011**, *31*, 285−311.

(6) Gibbons, S. E.; Wang, C.; Ma, Y. Determination of pharmaceutical and personal care products in wastewater by capillary electrophoresis with UV detection. *Talanta* **2011**, *84*, 1163−1168.

(7) Li, X.; Ying, G.-G.; Su, H.-C.; Yang, X.-B.; Wang, L. Simultaneous determination and assessment of 4-nonylphenol, bisphenol A and triclosan in tap water, bottled water and baby bottles. *Environ. Int.* **2010**, *36*, 557−562.

(8) Ren, L.; Fang, J.; Liu, G.; Zhang, J.; Zhu, Z.; Liu, H.; Lin, K.; Zhang, H.; Lu, S. Simultaneous determination of urinary parabens, bisphenol A, triclosan, and 8-hydroxy-2′-deoxyguanosine by liquid chromatography coupled with electrospray ionization tandem mass spectrometry. *Anal. Bioanal. Chem.* **2016**, *408*, 2621−2629.

(9) Regiart, M.; Magallanes, J. L.; Barrera, D.; Villarroel-Rocha, J.; Sapag, K.; Raba, J.; Bertolino, F. A. An ordered mesoporous carbon modified electrochemical sensor for solid-phase microextraction and determination of triclosan in environmental samples. *Sens. Actuators, B* **2016**, *232*, 765−772.

(10) Wu, T.; Li, T.; Liu, Z.; Guo, Y.; Dong, C. Electrochemical sensor for sensitive detection of triclosan based on graphene/palladium nanoparticles hybrids. *Talanta* **2017**, *164*, 556−562.

(11) Shaikh, N.; Taujale, S.; Zhang, H.; Artyushkova, K.; Ali, A.-M. S.; Cerrato, J. M. Spectroscopic Investigation of Interfacial Interaction of Manganese Oxide with Triclosan, Aniline, and Phenol. *Environ. Sci. Technol.* **2016**, *50*, 10978−10987.

(12) Han, X.; Tan, Z.; Huang, Z.; Chen, X.; Gong, Y.; Li, Q.; Xu, K.; Chen, D. Nondestructive detection of triclosan in antibacterial hand soaps using digitally labelled Raman spectroscopy. *Anal. Methods* **2017**, *9*, 3720−3726.

DOI: 10.1021/acsomega.8b03680
ACS Omega 2019, 4, 7931−7937

(13) Atar, N.; Eren, T.; Yola, M. L.; Wang, S. A sensitive molecular imprinted surface plasmon resonance nanosensor for selective determination of trace triclosan in wastewater. *Sens. Actuators, B* **2015**, *216*, 638−644.
(14) Ahn, K. C.; Ranganathan, A.; Bever, C. S.; Hwang, S. H.; Holland, E. B.; Morisseau, K.; Pessah, I. N.; Hammock, B. D.; Gee, S. J. Detection of the Antimicrobial Triclosan in Environmental Samples by Immunoassay. *Environ. Sci. Technol.* **2016**, *50*, 3754−3761.
(15) Lu, J.; Shi, Y.; Ji, Y.; Kong, D.; Huang, Q. Transformation of triclosan by laccase catalyzed oxidation: The influence of humic acid-metal binding process. *Environ. Pollut.* **2017**, *220*, 1418−1423.
(16) Nfodzo, P.; Choi, H. Triclosan decomposition by sulfate radicals: Effects of oxidant and metal doses. *Chem. Eng. J.* **2011**, *174*, 629−634.
(17) Sun, K.; Kang, F.; Waigi, M. G.; Gao, Y.; Huang, Q. Laccase-mediated transformation of triclosan in aqueous solution with metal cations and humic acid. *Environ. Pollut.* **2017**, *220*, 105−111.
(18) Guan, X.; He, D.; Ma, J.; Chen, G. Application of permanganate in the oxidation of micropollutants: a mini review. *Front. Environ. Sci. Eng.* **2010**, *4*, 405−413.
(19) Hu, L.; Martin, H. M.; Strathmann, T. J. Oxidation Kinetics of Antibiotics during Water Treatment with Potassium Permanganate. *Environ. Sci. Technol.* **2010**, *44*, 6416−6422.
(20) Jiang, J.; Pang, S.-Y.; Ma, J.; Liu, H. Oxidation of Phenolic Endocrine Disrupting Chemicals by Potassium Permanganate in Synthetic and Real Waters. *Environ. Sci. Technol.* **2012**, *46*, 1774−1781.
(21) Jiang, J.; Pang, S.-Y.; Ma, J. Role of Ligands in Permanganate Oxidation of Organics. *Environ. Sci. Technol.* **2010**, *44*, 4270−4275.
(22) Roderick, M. S.; Adcock, J. L.; Terry, J. M.; Smith, Z. M.; Parry, S.; Linton, S. M.; Thornton, M. T.; Barrow, C. J.; Francis, P. S. Chemiluminescence Evidence Supporting the Selective Role of Ligands in the Permanganate Oxidation of Micropollutants. *J. Phys. Chem. A* **2013**, *117*, 10286−10293.
(23) Chen, J.; Qu, R.; Pan, X.; Wang, Z. Oxidative degradation of triclosan by potassium permanganate: Kinetics, degradation products, reaction mechanism, and toxicity evaluation. *Water Res.* **2016**, *103*, 215−223.
(24) Jiang, J.; Pang, S.-Y.; Ma, J. Oxidation of Triclosan by Permanganate (Mn(VII)): Importance of Ligands and In Situ Formed Manganese Oxides. *Environ. Sci. Technol.* **2009**, *43*, 8326−8331.
(25) Thao, C. T. B.; Huy, B. T.; Sharipov, M.; Kim, J.-I.; Dao, V.-D.; Moon, J.-Y.; Lee, Y.-I. Yb^{3+},Er^{3+},Eu^{3+}-codoped YVO_4 material for bioimaging with dual mode excitation. *Mater. Sci. Eng., C* **2017**, *75*, 990−997.
(26) Chung, J. W.; Gerelkhuu, Z.; Oh, J. H.; Lee, Y.-I. Recent advances in luminescence properties of lanthanide-doped up-conversion nanocrystals and applications for bio-imaging, drug delivery, and optosensing. *Appl. Spectrosc. Rev.* **2016**, *51*, 678−705.
(27) Gerelkhuu, Z.; Jung, D.; The Huy, B.; Tawfik, S. M.; Conte, M. L.; Conte, E. D.; Lee, Y.-I. Highly selective and sensitive detection of catecholamines using $NaLuGdF_4$:Yb^{3+}/Er^{3+} upconversion nanoparticles decorated with metal ions. *Sens. Actuators, B* **2019**, *284*, 172−178.
(28) Gerelkhuu, Z.; Huy, B. T.; Sharipov, M.; Jung, D.; Phan, T.-L.; Conte, E. D.; Lee, Y.-I. One-step synthesis of $NaLu_{80-x}$ Gd_x F_4 :Yb_{18} $^{3+}$ /Er_2 $^{3+}$ (Tm^{3+}) upconversion nanoparticles for in vitro cell imaging. *Mater. Sci. Eng., C* **2018**, *86*, 56−61.
(29) Huy, B. T.; Gerelkhuu, Z.; Chung, J. W.; Dao, V.-D.; Ajithkumar, G.; Lee, Y.-I. Enhanced light harvesting with chromium in $NaLu_{0.70-x}Gd_{0.10}F_4$:$Yb_{0.18}Er_{0.02}Cr_x$ ($0 \leq x \leq 0.25$) upconversion system. *Mater. Sci. Eng., B* **2017**, *223*, 91−97.
(30) Liu, Q.; Feng, W.; Li, F. Water-soluble lanthanide upconversion nanophosphors: Synthesis and bioimaging applications in vivo. *Coord. Chem. Rev.* **2014**, *273*−*274*, 100−110.
(31) Lin, M.; Gao, Y.; Diefenbach, T. J.; Shen, J. K.; Hornicek, F. J.; Park, Y. I.; Xu, F.; Lu, T. J.; Amiji, M.; Duan, Z. Facial Layer-by-Layer Engineering of Upconversion Nanoparticles for Gene Delivery: Near-Infrared-Initiated Fluorescence Resonance Energy Transfer Tracking and Overcoming Drug Resistance in Ovarian Cancer. *ACS Appl. Mater. Interfaces* **2017**, *9*, 7941−7949.
(32) Wang, F.; Banerjee, D.; Liu, Y.; Chen, X.; Liu, X. Upconversion nanoparticles in biological labeling, imaging, and therapy. *Analyst* **2010**, *135*, 1839−1854.
(33) Deng, R.; Xie, X.; Vendrell, M.; Chang, Y.-T.; Liu, X. Intracellular Glutathione Detection Using MnO_2-Nanosheet-Modified Upconversion Nanoparticles. *J. Am. Chem. Soc.* **2011**, *133*, 20168−20171.
(34) Yuan, J.; Cen, Y.; Kong, X.-J.; Wu, S.; Liu, C.-L.; Yu, R.-Q.; Chu, X. MnO_2-Nanosheet-Modified Upconversion Nanosystem for Sensitive Turn-On Fluorescence Detection of H_2O_2 and Glucose in Blood. *ACS Appl. Mater. Interfaces* **2015**, *7*, 10548−10555.
(35) Silva, A. R. M.; Nogueira, J. M. F. New approach on trace analysis of triclosan in personal care products, biological and environmental matrices. *Talanta* **2008**, *74*, 1498−1504.
(36) Libansky, M.; Zima, J.; Barek, J.; Dejmkova, H. Construction of an Electrochemical Cell System Based on Carbon Composite Film Electrodes and its Application for Voltammetric Determination of Triclosan. *Electroanalysis* **2014**, *26*, 1920−1927.
(37) Wang, H.; Zhang, A.; Wang, W.; Zhang, M.; Liu, H.; Wang, X. Separation and Determination of Triclosan and Bisphenol A in Water, Beverage, and Urine Samples by Dispersive Liquid-Liquid Microextraction Combined with Capillary Zone Electrophoresis-UV Detection. *J. AOAC Int.* **2013**, *96*, 459−465.
(38) Li, B.; Qiu, Z.; Wan, Q.; Liu, Y.; Yang, N. β-cyclodextrin functionalized graphene nano platelets for electrochemical determination of triclosan. *Phys. Status Solidi A* **2014**, *211*, 2773−2777.
(39) Moyo, M.; Florence, L. R.; Okonkwo, J. O. Improved electrooxidation of triclosan at nano-zinc oxide-multiwalled carbon nanotube modified glassy carbon electrode. *Sens. Actuators, B* **2015**, *209*, 898−905.
(40) Vidal, L.; Chisvert, A.; Canals, A.; Psillakis, E.; Lapkin, A.; Acosta, F.; Edler, K. J.; Holdaway, J. A.; Marken, F. Chemically surface-modified carbon nanoparticle carrier for phenolic pollutants: Extraction and electrochemical determination of benzophenone-3 and triclosan. *Anal. Chim. Acta* **2008**, *616*, 28−35.
(41) Yola, M. L.; Atar, N.; Eren, T.; Karimi-Maleh, H.; Wang, S. Sensitive and selective determination of aqueous triclosan based on gold nanoparticles on polyoxometalate/reduced graphene oxide nanohybrid. *RSC Adv.* **2015**, *5*, 65953−65962.
(42) Yang, J.; Wang, P.; Zhang, X.; Wu, K. Electrochemical Sensor for Rapid Detection of Triclosan Using a Multiwall Carbon Nanotube Film. *J. Agric. Food Chem.* **2009**, *57*, 9403−9407.
(43) Zhang, H.; Huang, C.-H. Oxidative Transformation of Triclosan and Chlorophene by Manganese Oxides. *Environ. Sci. Technol.* **2003**, *37*, 2421−2430.
(44) Wang, Z.; Liu, C.; Chang, L.; Li, Z. One-pot synthesis of water-soluble and carboxyl-functionalized [small beta]-$NaYF_4$:Yb,Er(Tm) upconversion nanocrystals and their application for bioimaging. *J. Mater. Chem.* **2012**, *22*, 12186−12192.
(45) Zheng, C.; Zhao, J.; Bao, P.; Gao, J.; He, J. Dispersive liquid-liquid microextraction based on solidification of floating organic droplet followed by high-performance liquid chromatography with ultraviolet detection and liquid chromatography-tandem mass spectrometry for the determination of triclosan and 2,4-dichlorophenol in water samples. *J. Chromatogr. A* **2011**, *1218*, 3830−3836.
(46) Guimarães, I. C.; Rezende, C. C.; da Silva, J. A. F.; de Jesus, D. P. Simultaneous determination of free fluoride and monofluorophosphate in toothpaste by capillary electrophoresis with capacitively coupled contactless conductivity detection. *Talanta* **2009**, *78*, 1436−1439.

DOI: 10.1021/acsomega.8b03680
ACS Omega 2019, 4, 7931−7937